Weak itinerant-electron ferromagnetism in amorphous Fe-Ti alloys

1990 J. Phys.: Condens. Matter 2 3595

(http://iopscience.iop.org/0953-8984/2/15/015)

J. Phys.: Condens. Matter **2** (1990) 3595–3610. Printed in the UK

Weak itinerant-electron ferromagnetism in amorphous Fe–Ti alloys

K Sumiyama, H Yasuda and Y Nakamura†
Department of Metal Science and Technology, Kyoto University, Kyoto 606, Japan

Received 18 August 1989, in final form 30 October 1989

Abstract. In bulk $Fe_{1-x}Ti_x$ alloys prepared by facing-target-type sputtering, an amorphous phase was obtained for $0.25 < x < 0.75$. These alloys are ferromagnetic at low temperatures and the Curie temperature T_C decreases with increasing x and becomes zero at $x \simeq 0.6$. The ratio $\mu p/\mu s$ of the magnetic moment in the paramagnetic state and that at 4.2 K versus T_C plot (the Rhode–Wolfarth plot) becomes very large for low T_C. The square of magnetisation shows a $T^{4/3}$-dependence at low temperatures. Moreover, the thermomagnetic curve of the amorphous $Fe_{1-x}Ti_x$ alloys with $x = 0.5$–0.6 show no cusp at a low temperature, indicating no spin-glass ordering. Therefore the amorphous $Fe_{1-x}Ti_x$ alloys are classified as random weak itinerant-electron ferromagnets. With increase in x, the residual resistivity increases, whereas the temperature coefficient of resistivity (TCR) is negative at room temperature and its absolute value increases with increasing temperature as observed in many amorphous alloys. However, the magnetic contribution to the negative TCR is prominent for $x < 0.6$.

1. Introduction

Non-equilibrium alloys have been produced by energising and quenching procedures such as solid quenching, liquid quenching and vapour quenching (Turnbull 1981). During sputter deposition, which is a typical vapour-quenching method, a high-energy vapour solution is condensed onto a cold substrate and the surface diffusion of energised adatoms is restricted, if the substrate is a good heat sink (Thornton 1977). Using RF diode sputtering and diode magnetron sputtering we could not attain a sufficiently high deposition rate to obtain bulk magnetic materials and could not avoid plasma irradiation of the substrate. On the contrary, facing-target-type sputtering, in which two targets are arranged parallel facing their planes and the proper magnetic field is applied perpendicular to the target surfaces in order to enhance the magnetron motion of electrons and to confine the plasma region in the space between the target planes, gives quite a high deposition rate even for magnetic materials (Naoe *et al* 1980) and effectively reduces plasma irradiation of the substrate, minimising the substrate heating and Ar contamination.

In vapour-quenched transition-metal alloys, an amorphous phase has been often obtained in the concentration range involving intermetallic compounds, i.e. topologically close packed (TCP) phases, in their equilibrium phase diagrams (Hafner 1981). A typical example is a sputter-deposited $Fe_{1-x}Ti_x$ alloy system (Sumiyama *et al* 1986, Massalski *et al* 1986); an amorphous phase was obtained in a wide concentration range

† Present address: Department of Mechanical and System Engineering, Faculty of Science and Technology, Ryukoku University, Ohtsu 520, Japan.

0953-8984/90/153595 + 16 $03.50

Table 1. Sputtering conditions.

Background pressure	100 μPa
Ar gas pressure	1 mPa
Input power	1 kW
Magnetic field	
At the target centre	8 kA m^{-1}
At the target edge	12 kA m^{-1}
Substrate temperature	330 K
Substrate	Polyimide and glass
Deposition rate	1.7 nm s^{-1}

$0.25 < x < 0.75$, although a single amorphous phase has not been obtained by liquid quenching (Yoshitake *et al* 1989), ball milling (von Allmen and Blatter 1987), ion implantation (Follstaedt *et al* 1983) and ion mixing (Brenier *et al* 1985). The Fe-rich amorphous $Fe_{1-x}Ti_x$ alloys are ferromagnetic at low temperatures (Fukamichi and Gambino 1981, Sumiyama *et al* 1983). The concentration dependences of the Curie temperature and magnetic moment are quite different from those of the equilibrium alloys, while the hyperfine field and quadrupole splitting are similar to those of intermetallic compound phases with the same concentration (Sumiyama *et al* 1983, 1986).

Since amorphous Fe–Ti alloys may be a candidate for high-technology materials, such as hydrogen absorption materials and hydrogen filters (Nakamura 1984), detailed studies of their structure and physical properties are important. Recently we have prepared bulk Fe–Ti alloys by facing-target-type sputtering. In this paper we deal with the magnetic and Mössbauer properties of amorphous Fe–Ti alloys, in comparison with the previous results for amorphous Fe–Ti alloys produced by RF sputtering (Sumiyama *et al* 1983, 1986, Liou and Chien 1984, Chien and Liou 1985).

2. Experimental procedures

Using a facing-target-type sputtering equipment and composite-type targets we prepared alloy specimens about 50 μm thick on water-cooled substrates. The alloy concentration was adjusted by changing the ratio of the surface area of Fe and Ti plates. The sputtering conditions are listed in table 1. The electron probe micro-analysis (EPMA) was made for the determination of chemical compositions of sputter-deposited alloys. The concentration distribution over the surface and the concentration difference between the free-surface side and the substrate side were determined for some alloys, indicating a uniform concentration within the experimental error of about 1.5%. The x-ray diffraction measurements were done at 290 K by using Fe Kα radiations and a graphite monochromater. The magnetisation was measured between 4.2 and 290 K in magnetic fields up to 1.03 MA by using a torsion balance magnetometer. Mössbauer spectra were measured by a constant-acceleration-type spectrometer at 290 and 4.2 K. The electrical resistivity was measured with a DC four-probe method between 4.2 and 290 K.

3. Results

Figure 1 shows the x-ray diffraction patterns of $Fe_{1-x}Ti_x$ alloys. BCC diffraction peaks are predominant for Fe-rich and Ti-rich alloys, a halo pattern is detected in the central

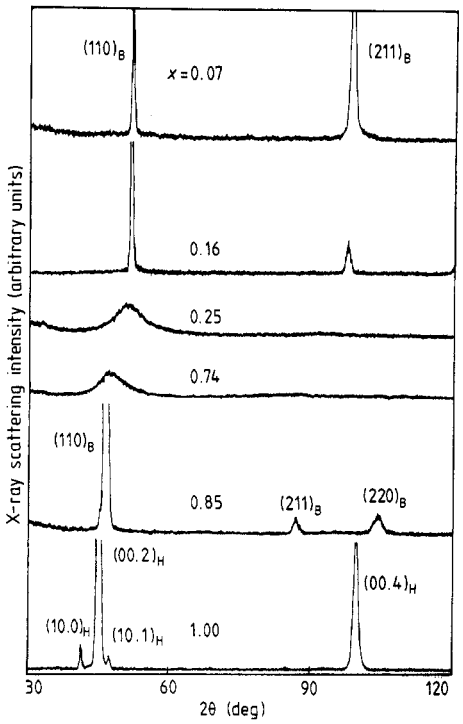

Figure 1. X-ray diffraction patterns of $Fe_{1-x}Ti_x$ alloys sputter deposited on water-cooled substrates.

concentration region, and HCP peaks occur in pure Ti. From these measurements, we have the non-equilibrium solubility diagram and the concentration dependence of lattice constants for the sputter-deposited $Fe_{1-x}Ti_x$ alloys as shown in figure 2. The α-Fe-type BCC phase is obtained for $x < 0.2$, an amorphous phase for $0.25 < x < 0.75$, the β-Ti-type BCC phase, which is a high temperature equilibrium phase, for $0.75 < x < 1.0$ (Massalski *et al* 1986), and the α-Ti-type HCP phase for $x = 1.0$. The lattice constant of the BCC alloys monotonically increases with increasing x, indicating a downward deviation from Vegard's law. The results shown in figure 2 agree with the previous results for $Fe_{1-x}Ti_x$ alloy films produced by an RF sputtering equipment (Sumiyama *et al* 1986), where their lattice constants are comparable with those of the bulk alloys (Pearson 1958).

The amorphous $Fe_{1-x}Ti_x$ alloys are ferromagnetic at low temperatures. In the magnetisation curves at 4.2 K shown in figure 3, the magnetisation σ increases with increasing magnetic field H, and its increasing rate is higher in the Ti-rich alloys. The spontaneous magnetic moment μ_s was estimated by linearly extrapolating the magnetisation curve at high fields to zero field and is shown as a function of x in figure 4. The value of μ_s monotonically decreases with increasing x and becomes zero at about $x = 0.6$, although it becomes zero at about $x = 0.4$ in amorphous $Fe_{1-x}Ti_x$ alloy films obtained by RF sputtering (Sumiyama *et al* 1983).

In the thermomagnetic curves for $Fe_{1-x}Ti_x$ alloys shown in figure 5, σ monotonically decreases with increasing temperature T. Figure 6 shows the σ^2 versus H/σ plot for amorphous $Fe_{1-x}Ti_x$ alloys, indicating that the straight lines are obtained at various temperatures and they are almost parallel in these alloys. The Curie temperature T_C of the amorphous $Fe_{1-x}Ti_x$ alloys obtained from these plots is shown as a function of x in figure 7. With increasing x, the value of T_C monotonically decreases and becomes zero at about $x = 0.6$. The values of T_C for the present $Fe_{1-x}Ti_x$ alloys roughly agree with the

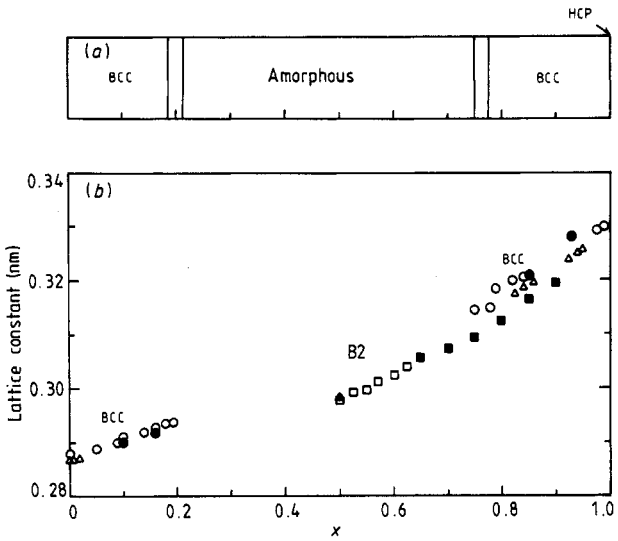

Figure 2. (*a*) Phase boundary diagram and (*b*) the lattice constants of $Fe_{1-x}Ti_x$ alloys: ●, the present alloys; ○, previous alloys (Sumiyama *et al* 1986) sputter-deposited on water-cooled substrates; ▲, B2-type ordered alloys (Pearson 1958); △, solid quenched alloys (Pearson 1958); □, B2-type ordered alloys obtained by liquid quenching (Ray *et al* 1972); ■, β-Ti-type BCC alloys obtained by liquid quenching (Ray *et al* 1972).

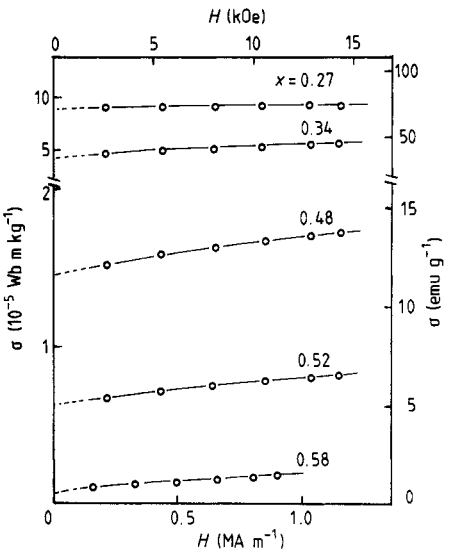

Figure 3. Magnetisation curves at 4.2 K of $Fe_{1-x}Ti_x$ alloys sputter deposited on water-cooled substrates.

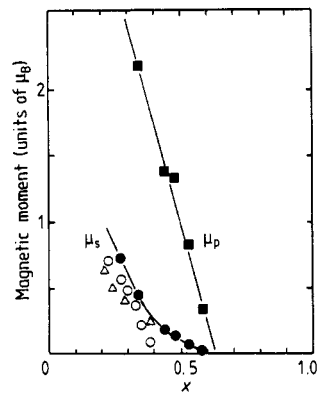

Figure 4. Magnetic moment μ_s at 4.2 K and magnetic moment μ_p in the paramagnetic state of amorphous $Fe_{1-x}Ti_x$ alloys sputter deposited on water-cooled substrates: ●, μ_s, present results; △, μ_s, after Fukamichi and Gambino (1981); ○, μ_s, previous results (Sumiyama *et al* 1983); ■, μ_p, present results.

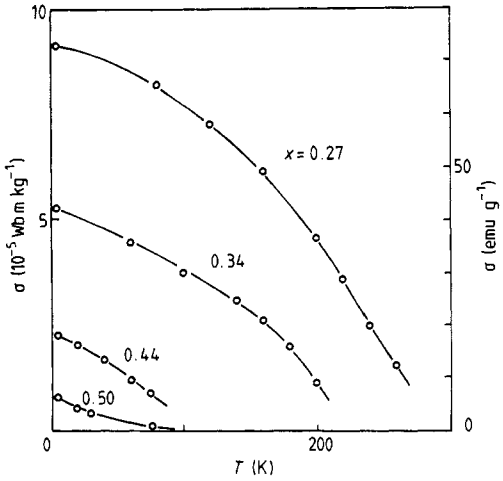

Figure 5. Thermomagnetic curves of amorphous $Fe_{1-x}Ti_x$ alloys in a magnetic field of 0.86 MA m^{-1}.

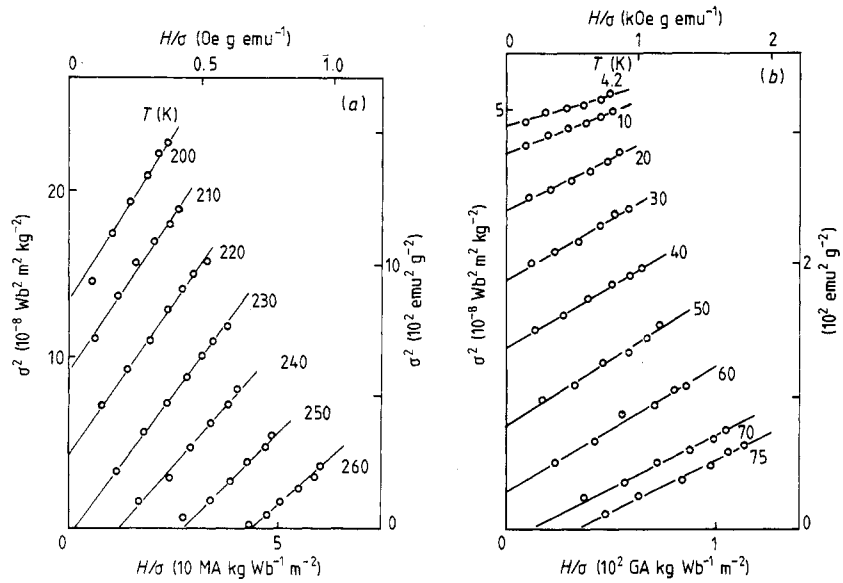

Figure 6. Square σ^2 of magnetisation versus H/σ plot (the Arrott plot) for amorphous $Fe_{1-x}Ti_x$ alloys in a magnetic field H up to 0.96 MA m^{-1}: (*a*) $x = 0.27$; (*b*) $x = 0.44$.

results obtained by Liou and Chien (1984), but their values and the critical concentration x_c of ferromagnetism are slightly higher than our previous results for the amorphous $Fe_{1-x}Ti_x$ alloy films obtained by RF sputtering (Sumiyama *et al* 1983).

Figure 8 shows the temperature dependence of the paramagnetic susceptibility χ and the inverse magnetic susceptibility $1/\chi$ for amorphous $Fe_{1-x}Ti_x$ alloys. Curie–Weiss-type behaviour is observed for $x < 0.5$, while the $1/\chi$ versus T plot is not straight, obeying

$$\chi = C/(T - \Theta_p) + \chi_s \tag{1}$$

for $0.5 < x < 0.6$, where C is the Curie–Weiss constant, $C = Ng^2\mu_B^2 S(S+1)/3k_B$ and Θ_p the paramagnetic Curie temperature and χ_s the Pauli paramagnetic susceptibility (N is the number of spin, g the g-value, μ_B the Bohr magneton and k_B the Boltzmann

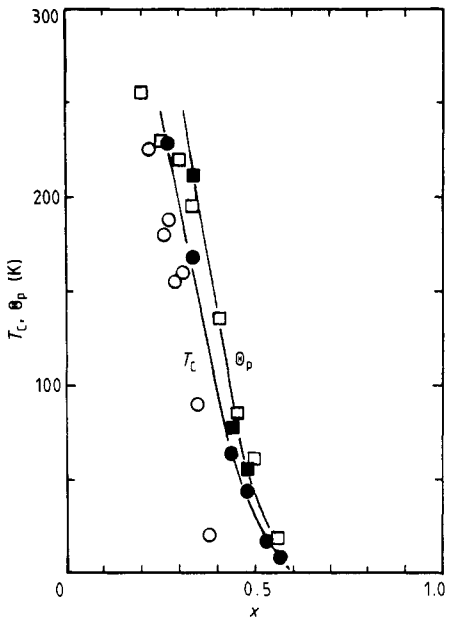

Figure 7. Curie temperature T_C estimated by the Arrott plot and paramagnetic Curie temperature Θ_p of amorphous $Fe_{1-x}Ti_x$ alloys sputter deposited on water-cooled substrates: ●, T_C, present results; ○, T_C, previous results (Sumiyama *et al* 1983); □, T_C after Liou and Chien (1984); ■, Θ_p, present results.

constant). The alloys with $x > 0.6$ are Pauli paramagnets. The magnetic moment in the paramagnetic state, $\mu_p = 2S$, and Θ_p are shown in figures 4 and 7, respectively. μ_p is much larger than μ_s, while Θ_p is slightly higher than T_C.

Figure 9 shows the temperature dependence of σ in a low magnetic field for amorphous $Fe_{0.5}Ti_{0.5}$ alloys; σ monotonically decreases with increasing temperature. No cusp is detectable even in the alloys near the critical concentration of ferromagnetism, x = 0.5–0.6.

Figure 10 shows the Mössbauer spectra at 290 K for amorphous $Fe_{1-x}Ti_x$ alloys. A doublet structure is ascribed to the quadrupole splitting and its broad half-width is due to a distribution of the electric field gradient. Each spectrum was fitted to a superposition of sets of two Lorentzians with different quadrupole splittings, where the half-width of each Lorentzian was assumed to be 0.25 mm s^{-1} (Sumiyama *et al* 1983). In order to get the best fitting, we also assumed a linear relation between the isomer shift (IS) and the quadrupole splitting (QS).

As shown in figure 11, the obtained distribution curves of QS cover the velocity range between 0 and 0.8 mm s^{-1}, which includes the QS values of $TiFe_2$ (C14), FeTi (B2) and Ti_2Fe ($E9_3$) phases (Wertheim and Wernick 1967, Wertheim *et al* 1969, Sumiyama *et al* 1986, 1987). The average QS value $\overline{QS}$ and the average IS value $\overline{IS}$ estimated from figures 10 and 11 are shown in figure 12. With increasing x, $\overline{QS}$ decreases for $x < 0.3$, exhibiting a shallow minimum around $x = 0.4$, and it gradually increases for $x > 0.4$ (Liou and Chien 1984, Sumiyama *et al* 1986), while the absolute average value of IS monotonically increases with increasing x. The values of QS and IS of the intermetallic compounds $TiFe_2$, FeTi and Ti_2Fe are different from those of the amorphous alloys with the same concentrations (Chien and Liou 1985).

Figure 13 shows Mössbauer spectra at 4.2 K for amorphous $Fe_{1-x}Ti_x$ alloys. A very broad ferromagnetic sextet indicates a distribution of the magnetic hyperfine field. Each spectrum was fitted to a superposition of sets of the six Lorentzians with different Zeeman splittings, where the half-width of the Lorentzians was assumed to be 0.25 mm s^{-1}, while the IS and the intensity ratio of the second and fifth peaks to the others were adjusted to

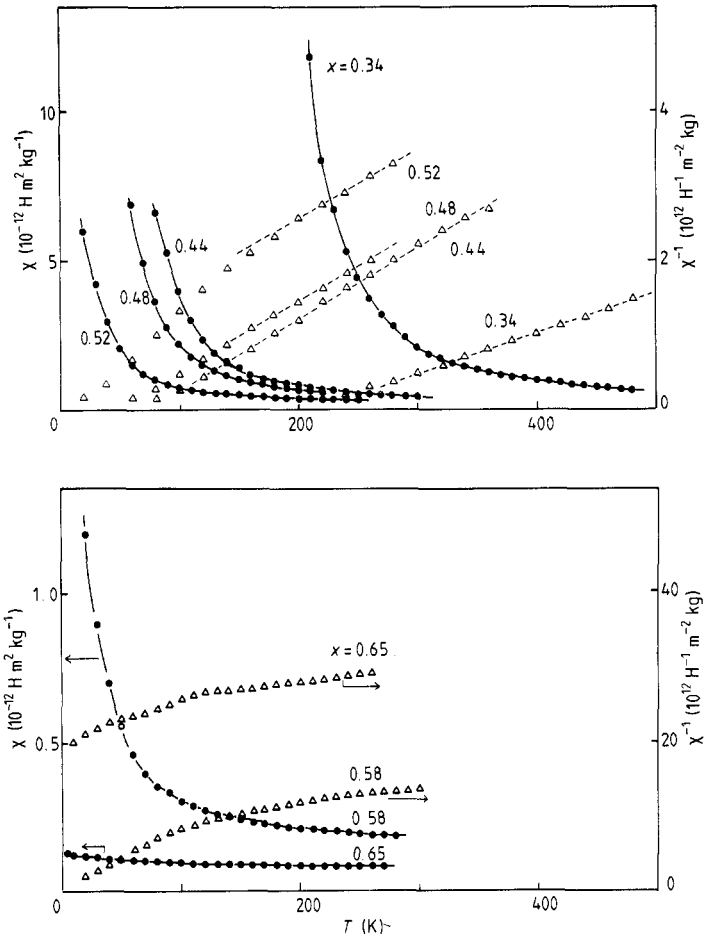

Figure 8. Temperature dependence of magnetic susceptibility χ and inverse magnetic susceptibility $1/\chi$ of amorphous $Fe_{1-x}Ti_x$ alloys in a magnetic field of 0.86 MA m^{-1}: (*a*) $x < 0.5$; (*b*) $x > 0.55$.

get the best fit. The contribution of the electric field gradient was neglected for simplicity. Figure 14 shows the obtained hyperfine field distribution curves. The high- and low-hyperfine-field components coexist for $x < 0.4$, while the low-field components dominate for $x > 0.4$. Figure 15 shows the average hyperfine field $\bar{H}_{hf}$ as a function of x. The value of $\bar{H}_{hf}$ monotonically decreases with increasing x and becomes zero at about $x = 0.5$ (Sumiyama *et al* 1983, Liou and Chien 1984). The critical concentration of ferromagnetism estimated from the Mössbauer measurements is slightly lower than that from the magnetic measurements.

Figure 16 shows the concentration dependence of the electrical resistivity $\rho(4.2\ K)$ at 4.2 K for amorphous $Fe_{1-x}Ti_x$ alloys. $\rho(4.2\ K)$ gradually increases with increasing x. Figure 17 shows the temperature dependence of the reduced electrical resistivity $\rho(T)/\rho(4.2\ K)$ for amorphous $Fe_{1-x}Ti_x$ alloys. The overall variation in $\rho(T)/\rho(4.2\ K)$ is about 5% between 4.2 and 290 K. With decreasing temperature, $\rho(T)/\rho(4.2\ K)$ of Fe-rich alloys increases below around T_C and reveals a maximum at T_M, while $\rho(T)/\rho(4.2\ K)$ of Ti-rich alloys also increases and exhibits a broad maximum at T_M. The temperature dependence of $\rho(T)/\rho(4.2\ K)$ in the present alloys almost agrees with the reported

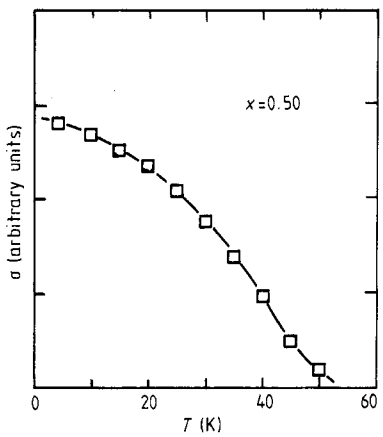

Figure 9. Thermomagnetic curve of amorphous $Fe_{0.5}Ti_{0.5}$ alloy near the critical concentration of ferromagnetism in a magnetic field of 16 kA m^{-1}.

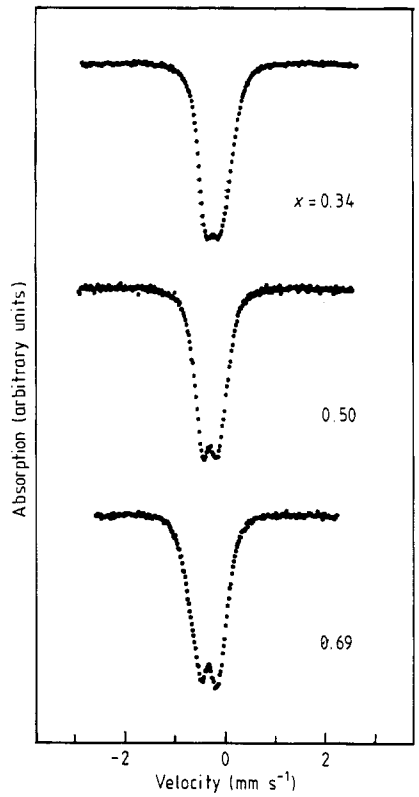

Figure 10. Mössbauer spectra at 290 K of amorphous $Fe_{1-x}Ti_x$ alloys sputter deposited on water-cooled substrates.

results (Chien and Liou 1984 and 1985, Fukamichi and Hiroyoshi 1985), except for the central concentration range $x = 0.4$–0.6.

4. Discussion

4.1. Structure

As shown in figure 2(*a*), the non-equilibrium phase boundary diagram of the sputter-deposited $Fe_{1-x}Ti_x$ alloys is almost the same as that of the previous sputter-deposited $Fe_{1-x}Ti_x$ alloy films (Sumiyama *et al* 1986), being insensitive to the sputtering method. This feature indicates that the amorphous Fe–Ti alloys are stable against the competing crystalline phases. The radial distribution functions of amorphous Fe–Ti alloys reveal a sharp first peak and a clear separation of the second and third peaks (Yasuda *et al* 1988). The coordination number of these alloys is about 11.5 and independent of the alloy concentration. Taking into account the extended x-ray absorption fine structure measurements (Yasuda *et al* 1990), the basic structure unit of the amorphous Fe–Ti alloys is an icosahedron, which is a dominant coordination polyhedron in the amorphous structure derived from the Bernal dense random packing of the hard-sphere model (Sumiyama *et al* 1986). Therefore the atomic configuration is random in the present amorphous $Fe_{1-x}Ti_x$ alloys.

As shown in figure 12, the average values of the QS of amorphous $Fe_{1-x}Ti_x$ alloys are different from those of the intermetallic compounds with the same alloy concentrations

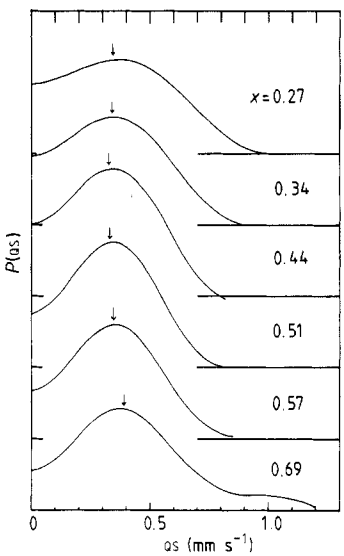

Figure 11. Distribution curves P(QS) of quadrupole splitting QS for amorphous $Fe_{1-x}Ti_x$ alloys sputter deposited on water-cooled substrates.

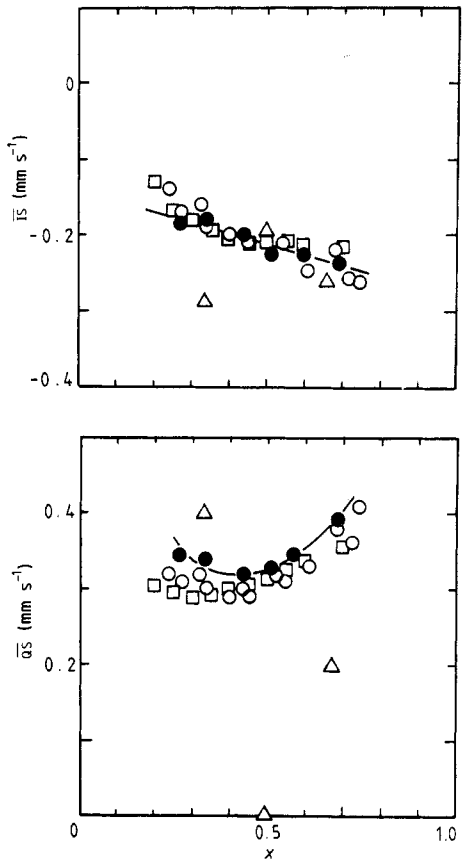

Figure 12. The average QS value $\overline{QS}$ and the average IS value $\overline{IS}$ for amorphous $Fe_{1-x}Ti_x$ alloys sputter deposited on water-cooled substrates: ●, present results; □, previous results (Liou and Chien 1984); ○, previous results (Sumiyama *et al* 1986); △, results on inter-metallic compounds (Wertheim and Wernick 1967, Wertheim *et al* 1969, Sumiyama *et al* 1987).

(Liou and Chien 1984). In figure 11, however, the wide range of QS distribution covers the QS values of the inter-metallic compounds (Wertheim and Wernick 1967, Wertheim *et al* 1969, Sumiyama *et al* 1986), indicating a wide variety of number, spacing and angle distributions of near neighbours around Fe atoms (Sumiyama *et al* 1986). In the present amorphous $Fe_{1-x}Ti_x$ alloys, the negative IS of the ^{57}Fe nucleus relative to α-Fe is due to electron donations from Ti atom sites to Fe atoms sites, while the decrease in the absolute value of IS corresponds to a decreased s-electron density which arises from the expansion of the s-electron wavefunction by adding larger Ti atoms (Wertheim *et al* 1969, van der Kraan and Buschow 1983).

4.2. Magnetism

In Fe–Ti alloys (Wertheim *et al* 1969, 1970, Gonser and Ron 1980), dilute Fe atoms are non-magnetic in HCP and BCC Ti matrices as well as in the B2-type ordered phase FeTi

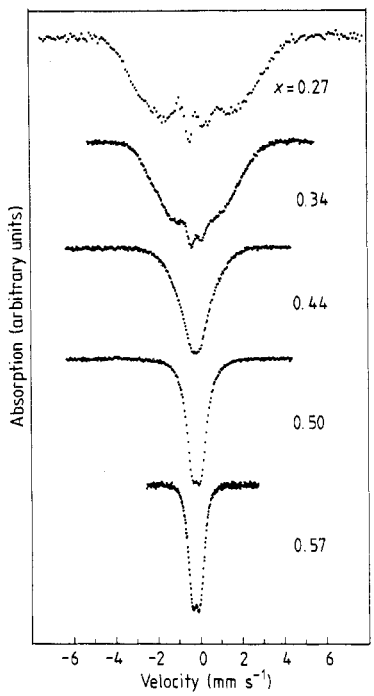

Figure 13. Mössbauer spectra at 4.2 K of amorphous $Fe_{1-x}Ti_x$ alloys sputter deposited on water-cooled substrates.

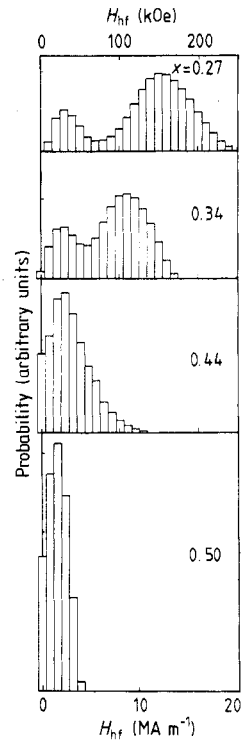

Figure 14. Distribution curves $P(H_{hf})$ of the hyperfine field H_{hf} for amorphous $Fe_{1-x}Ti_x$ alloys sputter deposited on water-cooled substrates.

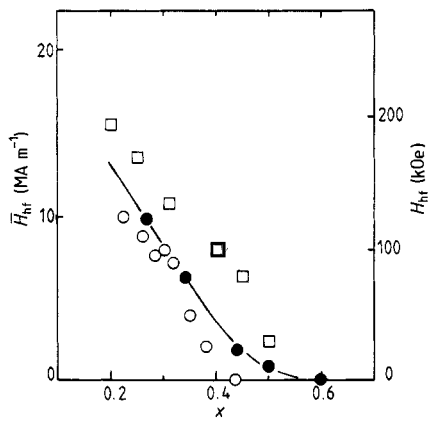

Figure 15. The average hyperfine field $\bar{H}_{hf}$ for amorphous $Fe_{1-x}Ti_x$ alloys sputter deposited on water-cooled substrates: ●, present results; ○, previous results (Sumiyama *et al* 1983); □, results after Liou and Chien (1984).

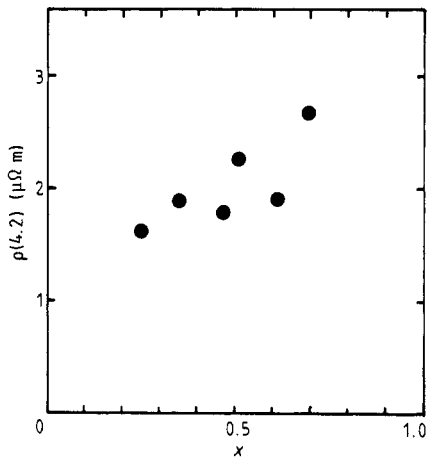

Figure 16. Concentration dependence of the electrical resistivity $\rho(4.2\ K)$ at 4.2 K for amorphous $Fe_{1-x}Ti_x$ alloys sputter deposited on water-cooled substrates.

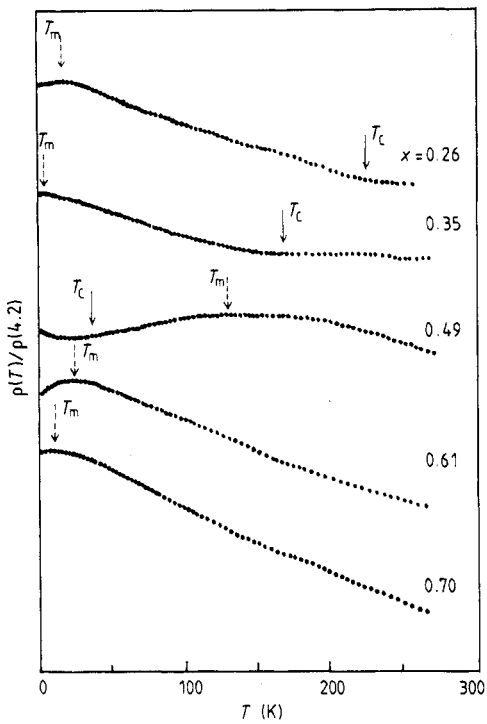

Figure 17. Temperature dependence of the reduced electrical resistivity $\rho(T)/\rho(4.2\,\mathrm{K})$ for amorphous $Fe_{1-x}Ti_x$ alloys sputter deposited on water-cooled substrates. The arrows indicate the Curie temperature T_C and the temperature T_M of the maximum of $\rho(T)/\rho(4.2\,\mathrm{K})$.

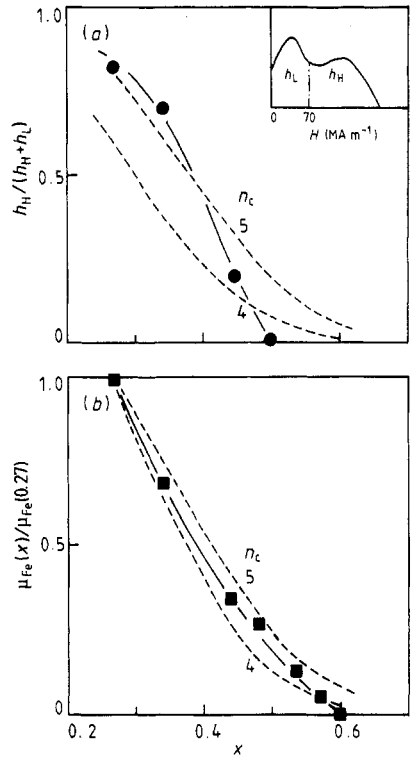

Figure 18. (*a*) Volume fraction $h_H/(h_H + h_L)$ of the high-hyperfine-field component in the amorphous $Fe_{1-x}Ti_x$ alloys: – – –, probabilities of Fe atoms with $n_c < 4$ and $n_c < 5$, where n_c is the critical number of nearest-neighbour Ti atoms for formation of a magnetic moment at Fe atom sites. (*b*) Concentration dependence of the reduced magnetic moment $\mu_{Fe}(x)/\mu_{Fe}(0.27)$ per Fe atom at 4.2 K: – – –, estimated values for $n_c < 4$ and $n_c < 5$, where these values are normalised by the values at $x = 0.27$.

where these Fe atoms are surrounded by a few or no nearest-neighbour Fe atoms. In the Laves phase, on the other hand, Fe atoms at the 2a site carry no magnetic moment and those at the 6h site carry a moment of about $0.3\mu_B$ (Nakamichi 1968, Wertheim *et al* 1969, 1970), although these two inequivalent sites have the same near neighbours, six Fe and six Ti atoms. The nearly stoichiometric and Ti-rich Laves phase alloys are antiferromagnetic, in which the magnetic moments of Fe atoms on the 6h-site layers ferromagnetically couple and those alternative layers couple antiferromagnetically. On the other hand, the Fe-rich Laves phase alloys are ferromagnetic, where the substituted Fe atom on a Ti site makes the neighbouring 2a-site Fe atoms magnetic and provides an additional path for a magnetic coupling between layers of 6h-site Fe atoms, resulting in a formation of magnetic clusters with a magnetic moment of about $2\mu_B$. Since the short-range atomic configuration of amorphous Fe–Ti alloys is high dense stackings similar to those of the Laves phase and the ordered phase, the number of Fe atoms with near-neighbour Fe atoms is retained, giving rise to ferromagnetism up to a Ti-richer concentration region in comparison with the Laves phase and ordered phase alloys and thus

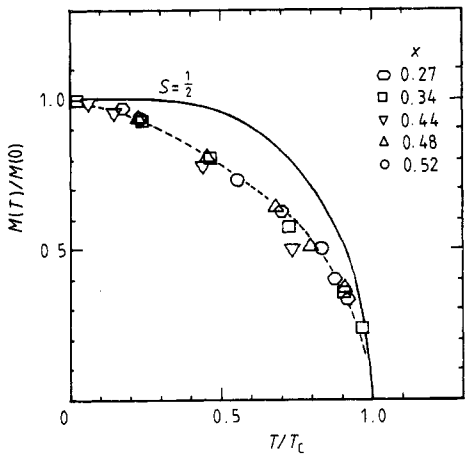

Figure 19. Reduced magnetisation $\sigma(T)/\sigma(0)$ versus reduced temperature T/T_C for amorphous $Fe_{1-x}Ti_x$ alloys sputter-deposited on water-cooled substrates, where T_C is the Curie temperature estimated by the Arrott plot. ——, Brillouin curve.

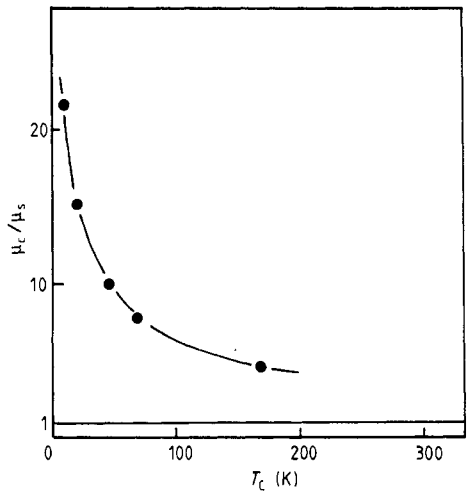

Figure 20. Ratio of magnetic moment μ_p in the paramagnetic state to the magnetic moment μ_s at 4.2 K as a function of the Curie temperature T_C for amorphous $Fe_{1-x}Ti_x$ alloys sputter-deposited on water-cooled substrates.

the ferromagnetism is stabilised in a wider concentration range in amorphous $Fe_{1-x}Ti_x$ alloys (Sumiyama *et al* 1983).

In figure 14, the distribution curve of H_{hf} shows double peaks, which have been commonly observed in Fe alloys with early transition-metal elements (Shiga and Nakamura 1978); the lower-hyperfine-field component h_L originates in Fe atoms carrying a small or no magnetic moment, and the higher-field component h_H in Fe atoms carrying a larger magnetic moment. Figure 18(*a*) shows the fraction $h_H/(h_L + h_H)$ of the number of Fe atoms with the high-hyperfine-field component for amorphous $Fe_{1-x}Ti_x$ alloys. On the assumption that the formation of the magnetic moment at Fe atom sites is influenced by the difference in the local atomic configuration around Fe atoms, the magnetic moment of Fe atoms is finite as the number n of nearest-neighbour Ti atoms is equal to or less than the critical number n_c and it becomes zero as n is more than n_c in random alloys. Here, the analysis of radial distribution function of amorphous $Fe_{1-x}Ti_x$ alloys indicates that the average coordination number $N = 11.5$ (Yasuda *et al* 1988) and the near-neighbour coordination polyhedron is similar to the icosahedron with $N = 12$; the binomial distribution function (Jaccarino and Walker 1965, Sumiyama *et al* 1983)

$$P = \sum_{n=0}^{n_c} {}_{12}C_n x^n (1-x)^{12-n} \tag{2}$$

gives the fraction P of Fe atoms carrying magnetic moments. As shown in figure 18(*b*), the values of P and $h_H(h_L + h_H)$ normalised by those at $x = 0.27$ are consistent for $n_c = 4$ and 5. The value of n_c for amorphous $Fe_{1-x}Ti_x$ alloys is smaller than $n_c = 6$ estimated for the amorphous $Fe_{1-x}Zr_x$ and $Fe_{1-x}Y_x$ alloys (Ishio *et al* 1988). Figure 19 shows the reduced magnetisation $\sigma(T)/\sigma(0)$ versus the reduced temperature T/T_C for amorphous $Fe_{1-x}Ti_x$ alloys. On increase in temperature, they decrease rapidly in comparison with the Brillouin function curve with $S = \frac{1}{2}$. Within the molecular-field approximation, the

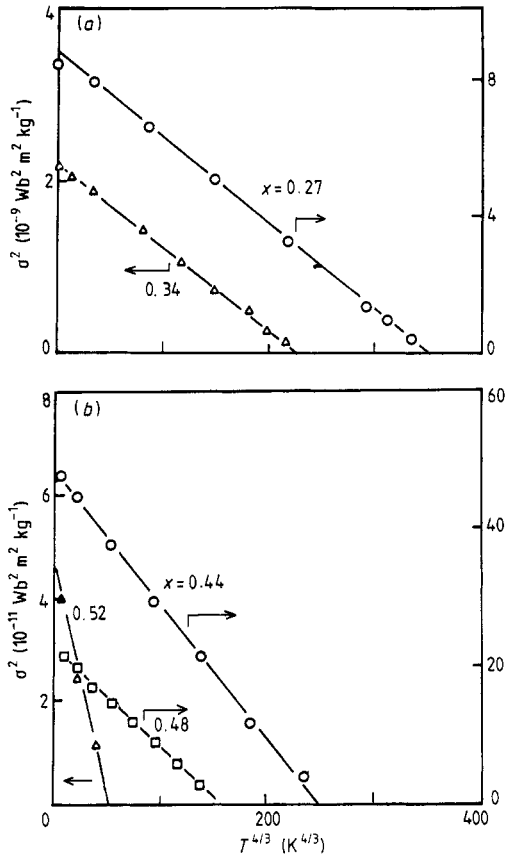

Figure 21. Square σ^2 of magnetisation versus $T^{4/3}$ plot for amorphous $Fe_{1-x}Ti_x$ alloys sputter-deposited on water-cooled substrates.

rapid reduction in magnetisation with increasing temperature can be ascribed to the fluctuation of the exchange field (Handrich 1969) $\Delta^2 = \langle(\Delta H_w)^2\rangle/\langle H_w\rangle^2$, where H_w is the molecular field, ΔH_w is the deviation of H_w from the average value $\langle H_w\rangle$ and the bracket $\langle\ \rangle$ means the average over the spatial distribution of H_w. In figure 19, $\Delta = 0.6$ for $x = 0.34$ and $\Delta = 0.5$ for $x = 0.5$ (Handrich 1969).

On the other hand, figure 20 shows μ_p/μ_s as a function of T_C (Rhodes and Wohlfarth 1963) for amorphous $Fe_{1-x}Ti_x$ alloys. The value of μ_p/μ_s is larger than unity and increases with decreasing T_C, indicating that amorphous $Fe_{1-x}Ti_x$ alloys belong to itinerant-electron ferromagnets. In figure 21, the square of magnetisation versus $T^{4/3}$ plots reveal straight lines in a wide temperature range. This temperature dependence is also a character of a very weak itinerant-electron ferromagnet (Moriya 1985). Moreover, the thermomagnetic curves show no spin-glass-like or cluster-glass-like cusp at low temperatures. In amorphous $Fe_{1-x}Ti_x$ alloys, the magnetic moment of Fe atoms is of an induced type and unstable so that these alloys are classified as random weak itinerant-electron ferromagnets.

4.3. Electrical resistivity

Electrical resistivities of vapour-quenched alloys are usually very large and are dominated by defect scattering. As shown in figure 16, the value of $\rho(4.2\ K)$ monotonically increase with increasing x, indicating a breakdown of the Nordheim rule (Ziman 1960).

In transition-metal alloys, the d electrons at the Fermi level E_F play the role of carriers in the electrical conductivity (Mizutani 1988). With increasing x, the density of states at E_F decreases and results in a reduction in the number of carriers.

In disordered transition-metal alloys, the temperature coefficient of resistivity (TCR) is positive for alloys with small values of $\rho(0)$ and becomes very small for $\rho(0) > 1\ \Omega$ m, while the TCR is negative for $\rho\ (0) > 1.5\ \Omega$ m (Mooij 1973). This empirical relation is roughly satisfied with the present amorphous $Fe_{1-x}Ti_x$ alloys as shown in figures 16 and 17.

According to a diffraction model (Cote and Meisel 1977, Mizutani 1988) the electrical resistivity $\rho\ (T)$, is expressed as

$$\rho(T) = [\rho(0) + \Delta\rho(T)] \exp[-2W(T)]. \tag{3}$$

Here, the exponential term (the Debye–Waller factor) is the resistivity due to quasi-elastic electron–phonon interactions and its low-temperature expansion results in the $1 - \alpha T^2$ temperature dependence of resistivity, leading to a reduction in the resistivity against temperature. $\rho(0)$ is the residual resistivity at 0 K and $\Delta\rho(T)$ is the resistivity caused by the inelastic electron–phonon interactions, giving rise to a positive TCR. Therefore the $\Delta\rho(T)$ term dominates and a positive TCR is observed in the whole temperature range for low-resistivity alloys, while the $\Delta\rho(T)$ term becomes less important relative to $\rho(0)$ term and the $\exp[-2W(T)]$ term gives rise to a negative TCR at high temperatures for high-resistivity alloys (Meisel and Cote 1984).

In the present amorphous $Fe_{1-x}Ti_x$ alloys, $\rho(0)$ monotonically increases from 1.5 to 2.5 $\mu\Omega$ m with increase in x, while $\rho(T)$ becomes temperature independent at high temperatures. In the framework of the diffraction theory, phonons with a wavelength exceeding the mean free path Λ, of conduction electrons are ineffective electron scatterers (saturation effect), because Λ is of the order of the inter-atomic spacing d for $\rho(0) > 1.0\ \mu\Omega$ m (Cote and Meisel 1978); the resistivity becomes temperature independent. Therefore, equation (2) describes the temperature dependence of $\rho(T)$ well for amorphous $Fe_{1-x}Ti_x$ alloys at high temperatures (Meisel and Cote 1984). However, at low temperatures, a peculiar temperature dependence is observed, in particular for $x < 0.5$. Since the latter alloys are ferromagnetic at low temperatures, the characteristic dependence may be related to the magnetic ordering.

In order to discuss the magnetic contribution to the electrical resistivity in the weak ferromagnetic alloys, we summarise the experimental results of the electrical resistivity in the Ni–Cu alloy system (Houghton *et al* 1970, Rossiter 1981), whose equilibrium phase diagram is of a homogeneous solid solution type. Ni-rich ferromagnetic alloys show a normal positive TCR and the spin-disorder resistivity, defined by

$$\rho_m(T) = \rho(T) - \rho_{ph}(T) - \rho(0) \tag{4}$$

increases with increasing temperature and saturates above the Curie temperature T_C, where $\rho_{ph}(T)$ is the resistivity due to the normal electron–phonon scattering process. On the contrary, Cu-rich alloys near the critical concentration of ferromagnetism show a negative TCR below about T_C of pure Ni (600 K) and reveal a large resistivity at 4.2 K (Rossiter 1981). If the linear dimension l_m of magnetic cluster (ferromagnetic polarisation cloud), is larger than Λ in the latter alloys, conduction electrons see bulk ferromagnetism within the clusters and ρ_m decreases from the paramagnetic value at low temperatures. On the other hand, if l_m is smaller than Λ, conduction electrons see a disordered array of large cluster moments and reveal a much larger magnetic cluster resistivity $\rho_{MC}(T)$ at low temperatures, while the inter-cluster magnetic correlations decrease and $\rho_{MC}(T)$ falls to the paramagnetic value of $\rho_m(T)$ at high temperatures.

As mentioned in the previous paragraph, the magnetic contribution to resistivity should decrease with decreasing temperature in amorphous $Fe_{1-x}Ti_x$ alloys, which are ferromagnetic at low temperatures and whose Λ are comparable with d. However, in amorphous $Fe_{1-x}Ti_x$ alloys, the value of H_{hf} markedly distributes in the ferromagnetic state, indicating a wide variety of magnetic moments μ_{Fe} at different Fe atom sites, depending upon the number of nearest-neighbour Fe atoms. Upon cooling amorphous $Fe_{1-x}Ti_x$ alloys from the room-temperature paramagnetic state, the magnetic polarisation clouds initially appear above T_C at the Fe sites surrounded by many Fe atoms and they incorporate as a uniform ferromagnet below T_C. In this process, conduction electrons see randomly distributed Fe atoms with different magnetic moments. Since μ_{Fe} increases at low temperatures, the magnetic contribution to the electrical resistivity increases. Even though this contribution is rather small in weak itinerant-electron ferromagnets, it apparently dominates the temperature dependence of $\rho(T)$ in high-resistivity alloys, where phonons with a long wavelength do not contribute to the electrical resistivity.

Acknowledgments

The authors wish to thank Mr R Iehara for his technical support and Mr T Unesaki for carrying out the EPMA. They are indebted to Mr S Kambara of Nippon Mining Co. Ltd and Mr M Suyama at Showa Denko Co. Ltd for supplying the Ti and Fe targets, respectively. This work was partially supported by a Grant-in-Aid for Developmental Scientific Research (Grant 60850132) given by the Ministry of Education, Science and Culture, Japan.

References

Brenier R, Perez A, Thevenard P, Treilleux M and Capra T 1985 *Mater. Sci. Eng.* **69** 83–8
Chien C L and Liou S H 1984 *J. Non-Cryst. Solids* **61–2** 1119–24
—— 1985 *Phys. Rev.* **31** 8238–41
Cote P J and Meisel L V 1977 *Phys. Rev. Lett.* **39** 102–5
—— 1978 *Phys. Rev. Lett.* **40** 1586–9
Follstaedt D M, Pope L E, Knapp J A, Picraux S T and Yost F G 1983 *Thin Solid Films* **107** 259–67
Fukamichi K and Gambino R J 1981 *IEEE Trans. Magn.* **MAG-17** 3059–61
Fukamichi K and Hiroyoshi H 1985 *Sci. Rep. Res. Inst. Tohoku Univ.* A **32** 154–67
Gonser U and Ron M 1980 *Applications of Mössbauer Spectroscopy* vol II ed R L Cohen (New York: Academic) pp 281–327
Hafner J 1981 *Glassy Metals* vol I ed H-J Güntherodt and H Beck (Berlin: Springer) pp 93–140
Handrich K 1969 *Phys. Status Solidi* **32** K55–8
Houghton R W, Sarachik M P and Kouvel J S 1970 *Phys. Rev. Lett.* **25** 238–9
Ishio S, Aubertin F, Limbach T, Engelman H, Dezsi L, Gonser U, Fries S, Takahashi M and Fujikura M 1988 *J. Phys. F: Met. Phys.* **18** 2253–63
Jaccarino V and Walker L R 1965 *Phys. Rev. Lett.* **15** 258–9
Liou S H and Chien C L 1984 *J. Appl. Phys.* **55** 1820–2
Massalski T B, Murray J L, Bennett L H, Baker H and Kacprzak L 1986 *Binary Alloy Phase Diagrams* (Metals Park, Ohio: American Society of Metals) pp 1117–9
Meisel L V and Cote P J 1984 *Phys. Rev.* B **34** 1743–53
Mizutani U 1988 *Mater. Sci. Eng.* **99** 165–73
Mooij J H 1973 *Phys. Status Solidi* a **17** 521–30
Moriya Y 1985 *Spin Fluctuations in Itinerant Electron Magnetism* (Berlin: Springer)
Nakamichi T 1968 *J. Phys. Soc. Japan* **25** 1189

Nakamura K 1984 *Scr. Metall.* **18** 793–7
Naoe M, Yamanaka S and Hoshi Y 1980 *IEEE Trans. Magn.* **MAG-16** 646–8
Pearson W B 1958 *A Handbook of Lattice Spacings and Structures of Metals and Alloys* (Oxford: Pergamon) pp 661–2
Ray R, Giessen B C and Grant N J 1972 *Metall. Trans.* **3** 627–9
Rhodes P and Wohlfarth E P 1963 *Proc. R. Soc.* A **273** 247–58
Rossiter P L 1981 *J. Phys. F: Met. Phys.* **11** 2105–18
Shiga M and Nakamura Y 1978 *J. Phys. F: Met. Phys.* **8** 177–90
Sumiyama K, Ezawa H and Nakamura Y 1986 *Phys. Status Solidi* a **93** 81–6
—— 1987 *Acta Metall.* **35** 1221–8
Sumiyama K, Hashimoto Y and Nakamura Y 1983 *Trans. Japan. Inst. Met.* **24** 61–5, 66–70
Thornton J A 1977 *Ann. Rev. Mater. Sci.* **7** 239–60
Turnbull D 1981 *Metall. Trans.* A **12** 695–708
van der Kraan A M and Buschow K H J 1983 *Phys. Rev.* B **27** 2693–7
von Allmen M and Blatter A 1987 *Appl. Phys. Lett.* **50** 1873–5
Wertheim G K and Wernick J H 1967 *Acta Metall.* **15** 297–302
Wertheim G K, Wernick J H and Sherwood R C 1969 *Solid State Commun.* **7** 1399–402
Wertheim G K, Buchanan D N E and Wernick J H 1970 *Solid State Commun.* **8** 2173–6
Yasuda H, Sumiyama K and Nakamura Y 1988 *Trans. Japan. Inst. Met. Suppl.* **29** 139–42
Yasuda H, Sumiyama K, Nakamura Y, Tanaka T and Yoshida S 1990 to be published
Yoshitake T, Kubo Y and Igarashi H 1989 private communication
Ziman J M 1960 *Electrons and Phonons* (Oxford: Clarendon) p 337